THE JOURNAL OF PHYSICAL CHEMISTRY Letters

Letter

pubs.acs.org/JPCL

Bilayer Phosphorene: Effect of Stacking Order on Bandgap and Its Potential Applications in Thin-Film Solar Cells

Jun Dai and Xiao Cheng Zeng*

Department of Chemistry and Department of Mechanical and Materials Engineering, University of Nebraska-Lincoln, 536 Hamilton Hall, Lincoln, Nebraska 68588, United States

Supporting Information

ABSTRACT: Phosphorene, a monolayer of black phosphorus, is promising for nanoelectronic applications not only because it is a natural p-type semiconductor but also because it possesses a layer-number-dependent direct bandgap (in the range of 0.3 to 1.5 eV). On basis of the density functional theory calculations, we investigate electronic properties of the bilayer phosphorene with different stacking orders. We find that the direct bandgap of the bilayers can vary from 0.78 to 1.04 eV with three different stacking orders. In addition, a vertical electric field can further reduce the bandgap to 0.56 eV (at the field strength 0.5 V/Å). More importantly, we find that when a monolayer of MoS_2 is superimposed with the p-type AA- or AB-stacked bilayer phosphorene, the combined trilayer can be an effective solar-cell material with type-II heterojunction alignment. The power conversion efficiency is predicted to be ∼18 or 16% with AA- or AB-stacked bilayer phosphorene, higher than reported efficiencies of the state-of-the-art trilayer graphene/transition metal dichalcogenide solar cells.

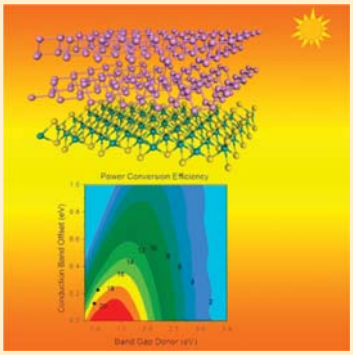

SECTION: Molecular Structure, Quantum Chemistry, and General Theory

Two-dimensional (2D) materials such as monolayer graphene and monolayer transition metal dichalcogenide (TMDC) MoS_2 have attracted intensive research interests owing to their fascinating electronic, mechanical, optical, or thermal properties, some of them not seen in their bulk counterparts, for example, the massless Dirac-fermion behavior of the graphene.[1−3] However, the lack of a bandgap in graphene severely limits its applications in nanotransistors.[4−6] Monolayer MoS_2 does possess a direct bandgap of ∼1.8 eV.[7] Indeed, the field effect transistor (FET) based on monolayer MoS_2 has demonstrated good device performance with a high on/off ratio of ∼10^8.[8,9] Nevertheless, although the carrier mobility in monolayer MoS_2 was previously reported[8] to be ∼200 $cm^2/V/s$ and may be further improved to 500 $cm^2/V/s$,[9] a few recent experiments indicate that the mobility values might be overestimated due to the capacitive coupling between the gates,[10,11] thereby limiting its wide application in electronics.

Very recently, a new 2D semiconducting material with a direct bandgap, namely, the few-layer black phosphorus (phosphorene), has been successfully isolated.[12−14] Moreover, the phosphorene-based FET exhibits high mobility of 286 $cm^2/V/s$ and appreciably high on/off ratios, up to 10^4.[13] The mobility is thickness-dependent and can be as high as ∼1000 $cm^2/V/s$ at ∼10 nm thickness.[12] Like graphite, black phosphorus, the bulk counterpart of phosphorene, is also a layered material with weak interlayer van der Waals (vdW) interaction. In the monolayer phosphorene, the phosphorus atom is bonded with three adjacent phosphorus atoms, forming a puckered honeycomb structure. (See Figure 1.) One of novel properties of the phosphorene is the thickness-dependent

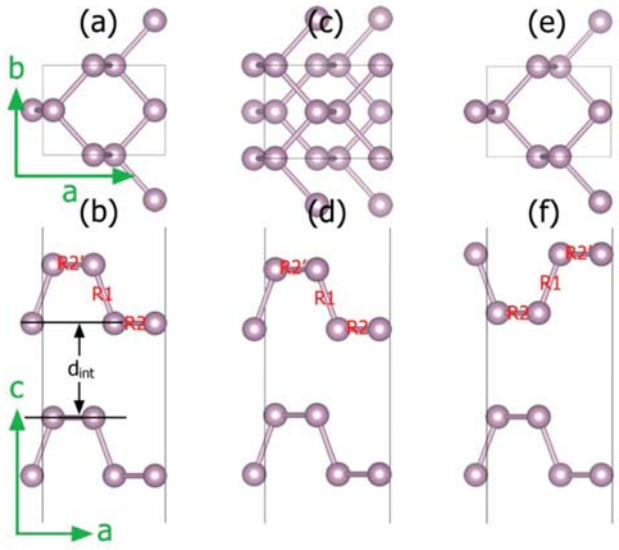

Figure 1. Three stacking structures of bilayer phosphorene. (a,c,e) Top view of AA-, AB-, and AC-stacking; (b,d,f) Side view of AA-, AB-, and AC-stacking. *R*1, *R*2, and d_{int} denote the two types of P−P bond length and interlayer distance, respectively.

Received: February 25, 2014
Accepted: March 24, 2014
Published: March 24, 2014

bandgap. Previous first-principles calculations show that the bandgap ranges from ∼1.5 eV for a monolayer to ∼0.6 eV for a five-layer.[15] Bulk black phosphorus, however, has a direct bandgap of 0.3 eV.[16−18] The bandgap of monolayer phosphorene is also predicted to be highly sensitive to either in-plane or out-of-plane strain. A ∼3% in-plane strain can change phosphorene from a direct-gap to an indirect-gap semiconductor,[13] while a vertical compression can induce the semiconductor to metal transition.[19] Because the electronic properties of phosphorene are highly dependent on its thickness, it is of both fundamental and practical interests to attain a better understanding of the effect of interlayer interaction on the electronic properties. Bilayer phosphorene is the thinnest multilayer system that can provide fundamental information on the interlayer interaction and stacking-dependent electronic and optical properties, a feature akin to the bilayer graphene systems.[20−23]

Three possible stacking orders of bilayer phosphorene are considered, namely, AA-, AB-, and AC-stacking. As shown in Figure 1a, for the AA-stacking, the top layer is directly stacked on the bottom layer. The AB-stacking can be viewed as shifting the bottom layer of the AA-stacking by half of the cell along either *a* or *b* direction (Figure 1c). As a result, the edge of the puckered hexagon of the top layer is located in the center of the puckered hexagon of the bottom layer. For the AC-stacking, the top and bottom layers are mirror images of each other. The computed structural parameters are listed in Table 1, where one

Table 1. Optimized Lattice Constants (*a* and *b*), Bond Length (*R*1, *R*2, and *R*2′), and the Nearest Distance between the Adjacent Layer (d_{int}) of Bilayer Phosphorene with Three Different Stacking Orders[a]

	a	*b*	*R*1	*R*2	*R*2′	d_{int}
AA	4.550	3.326	2.283	2.243	2.235	3.495
AB	4.526	3.331	2.277	2.242	2.238	3.214
AC	4.535	3.324	2.274	2.238	2.236	3.729

[a]Unit is angstroms.

can see that the lattice constants (*a* and *b*) and bond lengths (*R*1, *R*2, and *R*2′) differ slightly for different stacking order and *R*2 is always larger than *R*2′. The most notable difference among the three stacking orders is the nearest distance between the top and bottom layer (d_{int}), which varies from 3.214 Å in the AB-stacking to 3.729 Å in the AC-stacking. Our total-energy calculations based on the HSE06 hybrid functional indicate that the AB-stacking is energetically the most favorable, which is 8 and 7 meV/atom lower than that of AA- and AC-stacking, respectively.

The HSE06 electronic band structures of AA-, AB-, and AC-stacked bilayer phosphorene are shown in Figure 2a−c. Clearly, the direct-gap feature is retained regardless of the stacking order. Both the valence band maximum (VBM) and conduction band minimum (CBM) are located at the Γ point. Among the three bilayers with different stacking orders, the AB-stacked bilayer possesses the widest bandgap of 1.04 eV, while for the AA- and AC-stacked bilayers, the bandgap is 0.95 and 0.78 eV, respectively. By comparing the band structures, we find that the position of VBM with respect to the Fermi level is almost the same, while the CBM of AA- and AC-stacked bilayers is shifted downward compared with that of AB-stacked bilayer. To understand this difference in the CBM location, we plot the isosurfaces of the charge density corresponding to VBM and CBM of AA-, AB-, and AC-stacked bilayer phosphorene in Figure 2d−i, respectively. One can see that the VBM is contributed from the localized states of P atoms, while CBM is partially contributed from delocalized states, especially in the interfacial area between the top and bottom layers. Hence, different stacking-order results in different $\pi-\pi$ interaction distance between the delocalized states and thereby different interaction strength and bandgap.

Previous theoretical and experimental studies have shown that applying a vertical electric field can tune the bandgap of 2D bilayer graphene and MoS_2.[20,24−29] It is therefore interesting to see how bilayer phosphorene responses to a vertical electric field. The computed bandgap versus the external electric field for bilayer phosphorene with different stacking orders is plotted in Figure 3. Note that within the range of electric field strength considered, the feature of direct bandgap is still retained for all three bilayer phosphorene systems. In general, the bandgap decreases with increasing the external electric field. The AB-stacked bilayer phosphorene is less sensitive to the external electric field than other two bilayers, and its bandgap decreases from 1.04 eV at 0 V/Å to 0.92 eV at 0.5 V/Å, while the bandgap of AA-stacked bilayer phosphorene is 0.97 eV at 0 V/Å and 0.74 eV at 0.5 V/Å. The AC-stacked bilayer phosphorene is the most sensitive to the electric field, and its bandgap changes from 0.78 eV at 0 V/Å to 0.56 eV at 0.5 V/Å. The tunable range of bandgap for the bilayer phosphorene via the vertical electric field is similar to that for the TMDC MoS_2/MoX_2 heterobilayers.[29,30] All in all, combining the stacking order with electric field, the bandgap of bilayer phosphorene can be tuned in a relatively wide range of 0.56 to 1.04 eV, increasing the tunability for their potential application in nanoelectronics.

The fact that AA-, AB-, and AC-stacked bilayer phosphorene possesses direct bandgap of 0.97, 1.04 and 0.78 eV, respectively, suggests that the bilayer phosphorene with mixed stacking orders may be a very good candidate as solar cell donor materials. To investigate this feasibility, we compute the imaginary part of frequency-dependent dielectric function via summing over pairs of occupied and empty states without considering the local field effects, using HSE06 functional. Figure 4c shows the computed results of (ε_{xx}^2), one of the diagonal parts of the in-plane components, for AA-, AB-, and AC-stacked bilayer phosphorene. Strong peaks around 1 eV for AA- and AC-stacked bilayers and ∼1.4 eV for AB-stacked bilayer can be seen, all arising from the interband VBM-CBM transition. There are also peaks due to other interband transitions. Overall, the optical absorption is in a relatively wide range from 1 to 4 eV for AA- and AC-stacked bilayers and 1.4 to 4 eV for AB-stacked bilayer, a critical factor to enhance the efficiency of a solar cell. These results confirm that the bilayer phosphorene can potentially serve as donor materials.

From our HSE06 calculations, we find the CBM for AA-, AB-, and AC-stacked bilayer phosphorene are −4.13, −4.03, and −4.43 eV, respectively, and the corresponding VBMs are −5.10, −5.07, and −5.20 eV, respectively. If appropriate semiconducting acceptors with matching band alignment can be found, we can build thin-film photovoltaic systems with the bilayer phosphorene. On the basis of the same (HSE06) method, we find the CBM and VBM of monolayer MoS_2 are −4.25 and −6.27 eV, respectively, matching those of AA- and AB-stacked bilayer phosphorene with a type-II heterojunction alignment (Figure 4a,b). The upper limit of the power-conversion efficiency (PCE) η is estimated in the limit of 100%

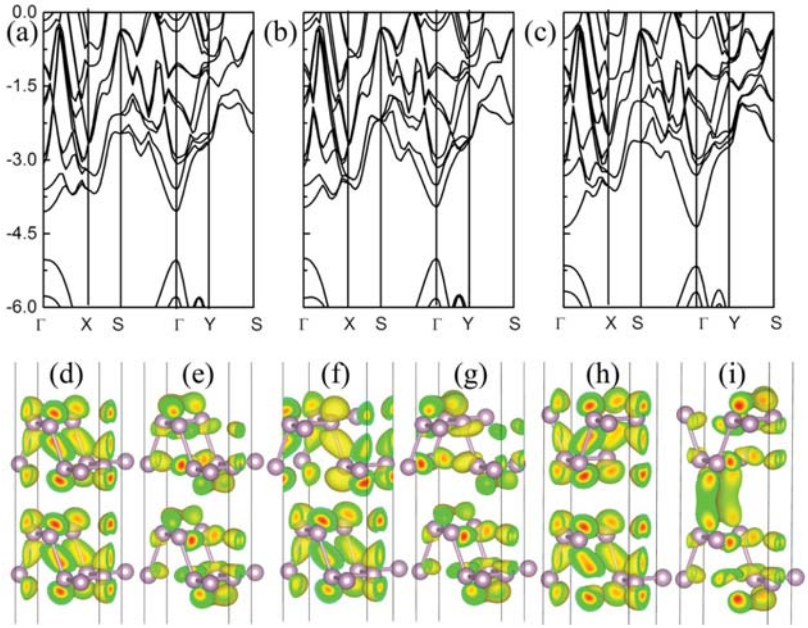

Figure 2. Computed band structures (based on HSE06) of (a) AA-, (b) AB-, and (c) AC-stacked bilayer phosphorene; (d,f,h) isosurface plot of the charge density corresponding to VBM for AA-, AB-, and AC-stacked bilayer phosphorene, while (e,g,i) are the charge density corresponding to the CBM for AA-, AB-, and AC-stacked bilayer phosphorene, respectively. The isovalue is 0.004 e/Bohr^3. Γ (0.0, 0.0, 0.0), X (0.0, 0.5, 0.0), S (0.5, 0.5, 0.0), and Y (0.5, 0.0, 0.0) refer to special points in the first Brillouin zone. The vacuum level is set to be 0 eV.

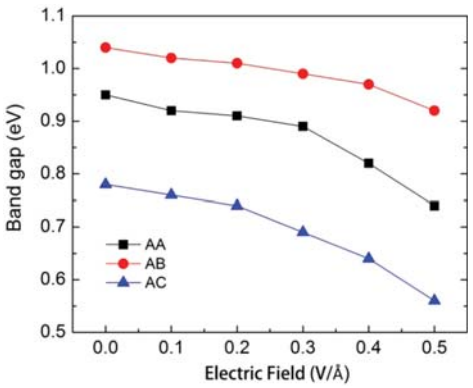

Figure 3. Field-dependent bandgaps of AA-, AB-, and AC-stacked bilayer phosphorene.

external quantum efficiency (EQE)[31,32] with the formula given by

$$\eta = \frac{J_{sc} V_{oc} \beta_{FF}}{P_{solar}} = \frac{0.65(E_g^d - \Delta E_c - 0.3) \int_{E_g}^{\infty} \frac{P(\hbar\varpi)}{\hbar\varpi} \, d(\hbar\varpi)}{\int_0^{\infty} P(\hbar\varpi) \, d(\hbar\varpi)}$$

where the band-fill factor (FF) is assumed to be 0.65, $P(\hbar\varpi)$ is taken to be the AM1.5 solar energy flux (expressed in W/m^{-2}/eV^{-1}) at the photon energy $\hbar\varpi$, and E_g^d is the bandgap of the donor, and the $(E_g^d - \Delta E_c - 0.3)$ term is an estimation of the maximum open circuit voltage V_{oc}. The integral in the numerator is the short circuit current J_{sc} in the limit of 100% EQE, and the integral in the denominator is the AM1.5 solar flux. As shown in Figure 4d, solar systems constructed with AA-/AB-stacked bilayer phosphorene and monolayer MoS_2 can achieve PCEs as high as ∼18/16%. These values are comparable to that of the PCBM/CBN system (10−20%)[30] and the recent predicted g-SiC_2-based systems (12−20%).[33] Although the proposed application in solar-cell systems is only three layers thin, thicker multilayers by stacking as the heterojunction could be a viable way to increase the interface area.

In conclusion, on the basis of DFT calculations, we investigate stacking effect on the electronic and optical properties of bilayer phosphorene. Our calculations show that CBM is very sensitive to the stacking order and can result in a change of the bandgap from 1.04 eV (AB-stacked) to 0.78 eV (AC-stacked). The bandgap also decreases with increasing the vertical electric field, for example, down to 0.56 eV at 0.5 V/Å field strength. Potential application of mixed bilayer phosphorene as a solar-cell donor material is examined. The predicted PCE for monolayer MoS_2/AA-stacked bilayer phosphorene and MoS_2/AB-stacked bilayer phosphorene can be as high as ∼18 and 16%, respectively, rendering the trilayer MoS_2 phosphorene a promising candidate in flexible optoelectronic devices. In view of the recent and successful fabrication of efficient thin-film solar cells using a van der Waals trilayer of graphene/TMDC WS_2/graphene by Novoselov and coworkers,[25] the trilayer phosphorene and TMDC MoS_2 systems may be also fabricated in the near future. We expect the van der Waals trilayer phosphorene/TMDC system is a more efficient solar cell than the trilayer graphene/TMDC systems[34,35] because the former can benefit from the absorption of wider range of wavelength in the solar spectrum, and the type-II heterojunction alignment can allow more efficient hole−electron separation.

■ COMPUTATIONAL METHODS

In the density functional theory (DFT) calculations, we adopt the generalized gradient approximation (GGA) for the exchange-correlation potential. The plane-wave cutoff energy for wave function is set to 500 eV. The ion−electron interaction is treated with the projected-augmented wave

dx.doi.org/10.1021/jz500409m | J. Phys. Chem. Lett. 2014, 5, 1289−1293

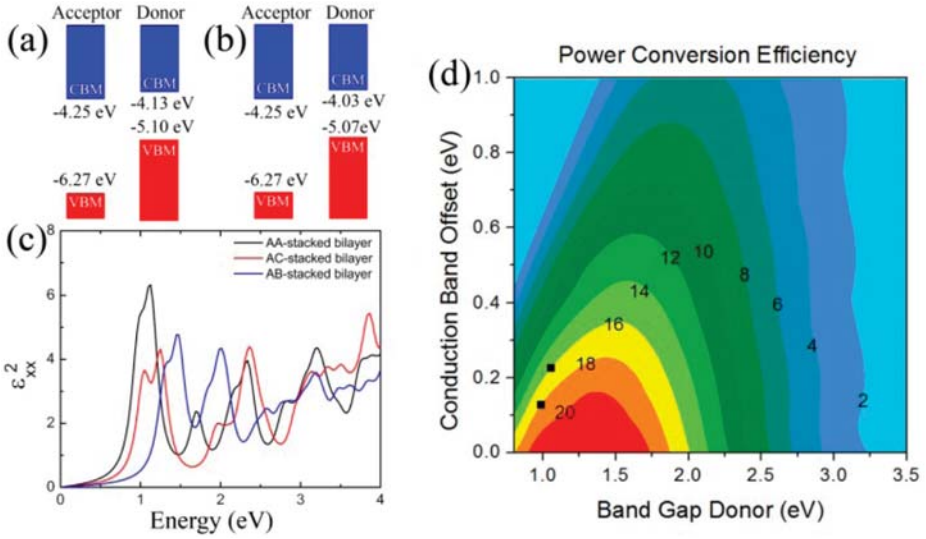

Figure 4. (a) Computed band offsets between monolayer MoS_2 (acceptor) and AA-stacked bilayer phosphorene (donor). (b) Band offsets between monolayer MoS_2 (acceptor) and AB-stacked bilayer phosphorene (donor). The numbers are the CBM and VBM levels with respect to vacuum level. (c) Computed imaginary part of the frequency-dependent dielectric function based on the HSE06 functional. (d) Computed power-conversion efficiency contour as a function of the donor bandgap and conduction band offset.

(PAW)[36,37] method as implemented in the Vienna ab initio simulation package (VASP 5.3).[38,39] For the geometry optimization, 8 × 10 × 4 and 8 × 10 × 1 Monkhorst-Pack *k*-meshes are adopted for the bulk phosphorus and bilayer phosphorene, respectively. A vacuum spacing of ∼15 Å is used so that the interaction between adjacent bilayers can be neglected. During the geometric optimization, both lattice constants and atomic positions are relaxed until the residual force on atoms are <0.01 eV/Å, and the total energy change is $<1.0 \times 10^{-5}$ eV. Previous theoretical calculations have shown that the vdW interaction must be accounted for to properly describe the geometrical properties of black phosphorus.[40] Also, previous theoretical calculations demonstrate that the geometrical and electronic properties of black phosphorus and few-layer phosphorene are highly functional dependent.[15,40] The combination of optB88-vdW[41,42] for geometry optimization and HSE06[43] for band structure calculation based on the optB88-vdW structure has been proven reliable for few-layer phosphorene systems.[15] Our benchmark calculation on bulk black phosphorus also confirms this combined DFT methods, which gives lattice constants of a = 4.475 Å, b = 3.337 Å, and c = 10.734 Å, in good agreement with both the experimental ones (a = 4.376 Å, b = 3.314 Å, and c = 10.478 Å)[44] and previous calculations.[15] Our HSE06 band structure calculation of black phosphorus also gives a direct bandgap of 0.36 eV (see Supporting Information Figure S1), in excellent agreement with the experimental bandgap of 0.3 eV.[16] In VASP, the vertical electric field is treated by adding an artificial dipole sheet in the unit cell.[45] Because the applied vertical electric field can affect the interlayer interaction within the bilayer phosphorene, the electronic structures of the systems are computed based on the fully relaxed geometry of the bilayer phosphorene under the vertical electric field.

■ ASSOCIATED CONTENT

Supporting Information

HSE06 band structures for bulk black phosphorus. This material is available free of charge via the Internet at http://pubs.acs.org.

■ AUTHOR INFORMATION

Corresponding Author

*E-mail: xzeng1@unl.edu.

Notes

The authors declare no competing financial interest.

■ ACKNOWLEDGMENTS

This work is supported by ARL (grant no. W911NF1020099), NSF (grant no. DMR-0820521), UNL Nebraska Center for Energy Sciences Research and Holland Computing Center, and a grant from USTC for (1000plan) Qianren-B summer research.

■ REFERENCES

(1) Novoselov, K.; Geim, A. K.; Morozov, S.; Jiang, D.; Grigorieva, M. K. I.; Dubonos, S.; Firsov, A. Two-Dimensional Gas of Massless Dirac Fermions in Graphene. *Nature* **2005**, *438*, 197−200.

(2) Novoselov, K.; McCann, E.; Morozov, S.; Fal'ko, V. I.; Katsnelson, M.; Zeitler, U.; Jiang, D.; Schedin, F.; Geim, A. Unconventional Quantum Hall Effect and Berry's Phase of 2π in Bilayer Graphene. *Nat. Phys.* **2006**, *2*, 177−180.

(3) Zhang, Y.; Tan, Y.-W.; Stormer, H. L.; Kim, P. Experimental Observation of the Quantum Hall Effect and Berry's Phase in Graphene. *Nature* **2005**, *438*, 201−204.

(4) Liao, L.; Lin, Y.-C.; Bao, M.; Cheng, R.; Bai, J.; Liu, Y.; Qu, Y.; Wang, K. L.; Huang, Y.; Duan, X. High-Speed Graphene Transistors with a Self-aligned Nanowire Gate. *Nature* **2010**, *467*, 305−308.

(5) Schwierz, F. Graphene Transistors. *Nat. Nanotechnol.* **2010**, *5*, 487−496.

(6) Wu, Y.; Lin, Y.-m.; Bol, A. A.; Jenkins, K. A.; Xia, F.; Farmer, D. B.; Zhu, Y.; Avouris, P. High-Frequency, Scaled Graphene Transistors on Diamond-like Carbon. *Nature* **2011**, *472*, 74−78.

(7) Mak, K. F.; Lee, C.; Hone, J.; Shan, J.; Heinz, T. F. Atomically Thin MoS_2: A New Direct-Gap Semiconductor. *Phys. Rev. Lett.* **2010**, *105*, 136805.
(8) Radisavljevic, B.; Radenovic, A.; Brivio, J.; Giacometti, V.; Kis, A. Single-Layer MoS_2 Transistors. *Nat. Nanotechnol.* **2011**, *6*, 147−150.
(9) Yoon, Y.; Ganapathi, K.; Salahuddin, S. How Good Can Monolayer MoS_2 Transistors be? *Nano Lett.* **2011**, *11*, 3768−3773.
(10) Fuhrer, M. S.; Hone, J. Measurement of Mobility in Dual-Gated MoS_2 Transistors. *Nat. Nanotechnol.* **2013**, *8*, 146−147.
(11) Radisavljevic, B.; Kis, A. Reply to 'Measurement of Mobility in Dual-Gated MoS_2 Transistors'. *Nat. Nanotechnol.* **2013**, *8*, 147−148.
(12) Li, L.; Yu, Y.; Ye, G. J.; Ge, Q.; Ou, X.; Wu, H.; Feng, D.; Chen, X. H.; Zhang, Y. Black Phosphorus Field-Effect Transistors. *Nat. Nanotechnol.* **2014**, DOI: 10.1038/nnano.2014.35.
(13) Liu, H.; Neal, A. T.; Zhu, Z.; Tomanek, D.; Ye, P. D. Phosphorene: An Unexpected 2D Semiconductor with a High Hole Mobility. *ACS Nano* **2014**, DOI: 10.1021/nn501226z.
(14) Reich, E. S. Phosphorene Excites Materials Scientists. *Nature* **2014**, *506* (7486), 19.
(15) Qiao, J.; Kong, X.; Hu, Z.-X.; Yang, F.; Ji, W. Few-Layer Black Phosphorus: Emerging Direct Band Gap Semiconductor with High Carrier Mobility. arXiv preprint arXiv:1401.5045, 2014.
(16) Warschauer, D. Electrical and Optical Properties of Crystalline Black Phosphorus. *J. Appl. Phys.* **1963**, *34*, 1853−1860.
(17) Asahina, H.; Morita, A. Band Structure and Optical Properties of Black Phosphorus. *J. Phys. C* **1984**, *17*, 1839.
(18) Takahashi, T.; Tokailin, H.; Suzuki, S.; Sagawa, T.; Shirotani, I. Electronic Band Structure of Black Phosphorus Studied by Angle-Resolved Ultraviolet Photoelectron Spectroscopy. *J. Phys. C* **1985**, *18*, 825.
(19) Rodin, A.; Carvalho, A.; Neto, A. Strain-induced Gap Modification in Black Phosphorus. arXiv preprint arXiv:1401.1801, 2014.
(20) Zhang, Y.; Tang, T.-T.; Girit, C.; Hao, Z.; Martin, M. C.; Zettl, A.; Crommie, M. F.; Shen, Y. R.; Wang, F. Direct Observation of a Widely Tunable Bandgap in Bilayer Graphene. *Nature* **2009**, *459*, 820−823.
(21) Wang, Y.; Ni, Z.; Liu, L.; Liu, Y.; Cong, C.; Yu, T.; Wang, X.; Shen, D.; Shen, Z. Stacking-Dependent Optical Conductivity of Bilayer Graphene. *ACS Nano* **2010**, *4*, 4074−4080.
(22) Kim, Y.; Yun, H.; Nam, S.-G.; Son, M.; Lee, D. S.; Kim, D. C.; Seo, S.; Choi, H. C.; Lee, H.-J.; Lee, S. W. Breakdown of the Interlayer Coherence in Twisted Bilayer graphene. *Phys. Rev. Lett.* **2013**, *110*, 096602.
(23) Zou, X.; Shang, J.; Leaw, J.; Luo, Z.; Luo, L.; Cheng, L.; Cheong, S.; Su, H.; Zhu, J.-X.; Liu, Y. Terahertz Conductivity of Twisted Bilayer Graphene. *Phys. Rev. Lett.* **2013**, *110*, 067401.
(24) Ohta, T.; Bostwick, A.; Seyller, T.; Horn, K.; Rotenberg, E. Controlling the Electronic Structure of Bilayer Graphene. *Science* **2006**, *313*, 951−954.
(25) Castro, E. V.; Novoselov, K.; Morozov, S.; Peres, N.; Dos Santos, J. L.; Nilsson, J.; Guinea, F.; Geim, A.; Neto, A. C. Biased Bilayer Graphene: Semiconductor with a Gap Tunable by the Electric Field Effect. *Phys. Rev. Lett.* **2007**, *99*, 216802.
(26) Oostinga, J. B.; Heersche, H. B.; Liu, X.; Morpurgo, A. F.; Vandersypen, L. M. Gate-Induced Insulating State in Bilayer Graphene Devices. *Nat. Mater.* **2007**, *7*, 151−157.
(27) Mak, K. F.; Lui, C. H.; Shan, J.; Heinz, T. F. Observation of an Electric-Field-Induced Band Gap in Bilayer Graphene by Infrared Spectroscopy. *Phys. Rev. Lett.* **2009**, *102* (25), 256405.
(28) Ramasubramaniam, A.; Naveh, D.; Towe, E. Tunable Band Gaps in Bilayer Transition-Metal Dichalcogenides. *Phys. Rev. B* **2011**, *84*, 205325.
(29) Lu, N.; Guo, H.; Lei, L.; Dai, J.; Wang, L.; Mei, W.-N.; Wu, X.; Zeng, X. C. MoS_2/MX_2 Heterobilayers: Bandgap Engineering via Tensile Strain or External Electrical Field. *Nanoscale* **2014**, *6*, 2879−2886.
(30) Lu, N.; Guo, H.; Wang, L.; Wu, X. J.; Zeng, X. C. van der Waals Trilayers and Superlattices: Modification of Electronic Structures of MoS_2 by Intercalation. *Nanoscale* **2014**, *6*, DOI: 10.1039/C4NR00783B.
(31) Bernardi, M.; Palummo, M.; Grossman, J. C. Semiconducting Monolayer Materials as a Tunable Platform for Excitonic Solar Cells. *ACS Nano* **2012**, *6* (11), 10082−10089.
(32) Scharber, M. C.; Mühlbacher, D.; Koppe, M.; Denk, P.; Waldauf, C.; Heeger, A. J.; Brabec, C. J. Design Rules for Donors in Bulk-heterojunction Solar Cells—Towards 10% Energy-conversion Efficiency. *Adv. Mater.* **2006**, *18*, 789−794.
(33) Zhou, L.-J.; Zhang, Y.-F.; Wu, L.-M. SiC_2 Siligraphene and Nanotubes: Novel Donor Materials in Excitonic Solar Cell. *Nano Lett.* **2013**, *13*, 5431−5436.
(34) Bernardi, M.; Palummo, M.; Grossman, J. C. Extraordinary Sunlight Absorption and One Nanometer Thick Photovoltaics Using Two-Dimensional Monolayer Materials. *Nano Lett.* **2013**, *13*, 3664−3670.
(35) Britnell, L.; Ribeiro, R.; Eckmann, A.; Jalil, R.; Belle, B.; Mishchenko, A.; Kim, Y.-J.; Gorbachev, R.; Georgiou, T.; Morozov, S. Strong Light-matter Interactions in Heterostructures of Atomically Thin Films. *Science* **2013**, *340*, 1311−1314.
(36) Blöchl, P. E. Projector Augmented-Wave Method. *Phys. Rev. B* **1994**, *50*, 17953.
(37) Kresse, G.; Joubert, D. From Ultrasoft Pseudopotentials to the Projector Augmented-Wave Method. *Phys. Rev. B* **1999**, *59*, 1758.
(38) Kresse, G.; Furthmüller, J. Efficient Iterative Schemes for Ab Initio Total-Energy Calculations Using a Plane-Wave Basis Set. *Phys. Rev. B* **1996**, *54*, 11169.
(39) Kresse, G.; Furthmüller, J. Efficiency of Ab-initio Total Energy Calculations for Metals and Semiconductors Using a Plane-Wave Basis Set. *Comput. Mater. Sci.* **1996**, *6*, 15−50.
(40) Appalakondaiah, S.; Vaitheeswaran, G.; Lebegue, S.; Christensen, N. E.; Svane, A. Effect of van der Waals Interactions on the Structural and Elastic Properties of Black Phosphorus. *Phys. Rev. B* **2012**, *86*, 035105.
(41) Dion, M.; Rydberg, H.; Schröder, E.; Langreth, D. C.; Lundqvist, B. I. Van der Waals Density Functional for General Geometries. *Phys. Rev. Lett.* **2004**, *92*, 246401.
(42) Klimeš, J.; Bowler, D. R.; Michaelides, A. Van der Waals Density Functionals Applied to Solids. *Phys. Rev. B* **2011**, *83*, 195131.
(43) Heyd, J.; Scuseria, G. E.; Ernzerhof, M. Erratum: "Hybrid Functionals Based on a Screened Coulomb Potential" [J. Chem. Phys. 118, 8207 (2003)]. *J. Chem. Phys.* **2006**, *124*, 219906.
(44) Brown, A.; Rundqvist, S. Refinement of the Crystal Structure of Black Phosphorus. *Acta Crystallogr.* **1965**, *19*, 684−685.
(45) Neugebauer, J.; Scheffler, M. Adsorbate-Substrate and Adsorbate-Adsorbate Interactions of Na and K Adlayers on Al (111). *Phys. Rev. B* **1992**, *46*, 16067.